Microscopic Mechanisms of Matrix Assisted Laser Desorption of Analyte Molecules: Insights from Molecular Dynamics Simulation

Tatiana E. Itina,[†] Leonid V. Zhigilei,[‡] and Barbara J. Garrison*[,†]

Department of Chemistry, 152 Davey Laboratory, The Pennsylvania State University, University Park, Pennsylvania 16802, and Department of Material Science and Engineering, Thornton Hall, University of Virginia, Charlottesville, Virginia 22903

Received: July 18, 2001; In Final Form: October 23, 2001

A hybrid model, which combines a bead-and-spring approach with the breathing sphere model, is developed for a molecular dynamics study of matrix-assisted laser desorption of analyte molecules. The combined model is used to investigate the initial stage of analyte molecular ejection at different laser fluences. Analyte molecules embedded near the irradiated surface are lifted off at laser fluences corresponding to the ablation threshold. Higher fluences are required to eject analyte molecules embedded deeper below the surface. At all considered laser fluences, analyte molecules are ejected within matrix clusters, thus solvated. The degree of solvation decreases with increasing laser fluence and during the ablation plume expansion. Possible mechanisms of analyte desolvation in the ejected plume are discussed. Analyte fragmentation is found to be negligible under all explored conditions.

1. Introduction

During the past decade, matrix-assisted laser desorption ionization (MALDI) has been recognized to be a powerful tool for mass-spectrometric analysis of large organic molecules such as proteins and peptides.[1−14] The MALDI technique is based on the embedding of analyte molecules into a solid matrix of molecules that strongly absorb laser irradiation. Laser excitation of the matrix molecules results in the ejection of the irradiated material and in the formation of an ablation plume. Analyte molecules are entrained in the plume and are usually detected in the form of ions. It was demonstrated in several experiments that under optimized conditions analyte molecules as heavy as 1.5 MDa are lifted off intact in MALDI.[12] The detection of the ejected high molecular weight molecules that have survived the ejection process without major fragmentation is the main advantage of MALDI as compared to other mass-spectrometric techniques. Therefore, MALDI has found many applications in the pharmaceutical industry and medical research.

Processes similar to the ones in MALDI have been recently utilized for the deposition of polymer thin films. Polymers are dissolved in an absorbing matrix instead of organic molecules. The laser ejected polymer molecules are captured on a surface, thus creating the thin polymer film with minimal fragmentation. This new technique is called matrix assisted pulsed laser evaporation (MAPLE).[15]

Several theoretical and numerical investigations of MALDI have been performed.[16−21] The attempts to understand MALDI mechanisms have raised many fundamental questions. One of the major questions is how large fragile molecules can survive the laser heating and subsequent ejection. To understand why analyte molecules do not dissociate during MALDI, many possible scenarios of the matrix disintegration and analyte liberation have been proposed.[5−7,17,22,23] These scenarios include disintegration via a nonequilibrium phase transition,[22] mechanical stress and shock,[17] and photofragmentation.[23] In addition, several models such as the cluster model[5−7] and "cool plume model"[17] have been elaborated to explain the MALDI process. The recent numerical prediction[20,21] and experimental observation[24] of cluster ejection during ablation has provided new information concerning the role of molecular clusters in MALDI.

In several papers, the molecular dynamics simulation technique was used for the analysis of MALDI.[16,18,25−29] For example, analyte ejection was studied using a detailed atomistic simulation.[16,18,19,25,26] Energy transfer rates from matrix to analyte molecules were investigated, and the ejection of analyte molecules was demonstrated.[16,25] The effect of burial depth of the analyte molecules on their ejection was also shown.[25] In addition, conformational changes of the analyte molecules have been recently studied by atomistic simulations.[26]

The atomistic approach, however, imposes a limitation on the system size and does not allow simulation with realistic laser penetration depth, pulse width, and fluence. To address these shortcomings, the breathing sphere model was designed.[27,28,30,31] The main advantage of this model is its ability to study the dynamics of the system at the mesoscopic length scale and therefore with more realistic laser properties. This new model has yielded a wealth of information on the microscopic mechanisms of laser ablation, the parameters of the ejected plume (velocity distributions of matrix and analyte molecules[27−29] and cluster ejection[20,27,28,32]), and their dependence on the irradiation conditions.[20,32] For example, the simulations have revealed the existence of a threshold fluence at which the transition from the desorption regime to the ablation regime takes place.[20,32] In addition, the ejection of analyte molecules was examined,[27−29] and the mass dependence of the velocity distribution of analyte molecules in matrix-assisted laser desorption was analyzed. In these simulations, however, the analyte molecules were represented by spheres without internal structure.

Several issues, such as the ejection of analyte molecules with an internal structure, have not been addressed within the

* To whom correspondence should be addressed. E-mail: bjg@psu.edu.
[†] The Pennsylvania State University.
[‡] University of Virginia.

10.1021/jp0127768 CCC: $22.00
Published on Web 12/11/2001

breathing sphere model. Herein, we present the results of a molecular dynamics (MD) simulation of laser ablation where the target material is modeled as a solid solution of analyte molecules in a molecular matrix. The analyte molecules are described using a bead-and-spring model,[34−36] where each bead represents one or several units of the macromolecule. The combination of the bead−spring model with the breathing sphere model is developed in order to provide new insights into the processes in MALDI of large molecules. Because united-atom models are used both for molecular matrix and for analyte molecules, the system size is significantly larger than in atomic-level models.[16−18,36] The new combined model is used to investigate the structural modifications of the molecules during the ejection. The role of molecular clusters and the degree of analyte solvation are examined. The possible mechanisms of the liberation of analyte molecules from clusters of matrix molecules (desolvation) are discussed further.

2. Model and Simulation Details

In the present section, we briefly review the basic features of the breathing sphere model developed for MD simulations of laser ablation of organic solids[20,27,28] and describe the coupling with the bead-and-spring model[33,34] used for the analyte molecules. In the breathing sphere model, each matrix molecule (or group of atoms) is represented by a single particle that has the true translational degrees of freedom but an approximate internal degree of freedom. The Langrangian that describes the motion in the system is given by

$$L = 1/2\sum_i m_i (dr_i/dt)^2 - \sum_{ij} U_r + 1/2\sum_i M_i (dR_i/dt)^2 - \sum_i U_R \quad (1)$$

where m_i, r_i, and R_i are the mass, position, and radius of the ith breathing sphere molecule.

The intermolecular forces among matrix molecules represent the van der Waals interaction in the molecular system. The Morse potential is chosen to represent the intermolecular interaction as follows:

$$U_r = \epsilon_n[\exp\{-2\alpha(r_{ij} - d_0)\} - 2\exp\{-\alpha(r_{ij} - d_0)\}] \quad (2)$$

where $r_{ij} = |r_i - r_j| - R_i - R_j$, i.e., the distance between the edges of breathing spheres. For the simulation presented in this paper, we have set $d_0 = 3$ Å, $\epsilon_n = 0.1$ eV, and $\alpha = 1$ Å^{-1}. A mass, m, of 100 Da is attributed to each matrix molecule. The cohesive energy of the molecular matrix is $\epsilon_c = 0.6$ eV, the elastic bulk modulus is on the order of 5 GPa, and the density is 1.2 g/cm^3. The parameters are chosen to model a generic molecular solid.

An internal degree of freedom is attributed to each molecule by allowing the spheres representing the matrix molecules to change their sizes or "breath". The frequency of the internal breathing mode is controlled by the parameters of the anharmonic potential ascribed to the internal degree of freedom

$$U_R = k_1\Delta R_i^2 + k_2\Delta R_i^3 + k_1\Delta R_i^4 \quad (3)$$

where $\Delta R_i = R_i - R_i^0$. The parameters of the internal potential determine the coupling between internal and translational molecular motion. In the present calculations, the equilibrium radius, R_i^0, is 1.4 Å. The parameters of the internal potential (k_1 = 30 eV/Å^2, $k_2 = -60$ eV/Å^3, and $k_3 = 60$ eV/Å^4) are chosen to provide the characteristic relaxation time of an excited molecule to be on the order of 10 ps.

The analyte molecules are modeled using a chain of beads and springs. Each bead represents one unit of analyte macromolecule. The chains are assumed to be flexible. For bonded interactions in analyte molecules, we use a Morse potential given by

$$U_p(l) = A[e^{-2B(l-l_0)} - 2e^{-B(l-l_0)}] \quad (4)$$

where l_0 is the equilibrium spring length and A is the potential well depth (dissociation energy). In simulations presented in this paper, $l_0 = 1.64$ Å and $A = 4.6$ eV. The stretching constant is assumed to be $k_{str} = 8.42$ eV/Å^2, and then $B = (k_{str}/2A)^{1/2} = 0.96$ Å^{-1}. The mass of each bead is set to be 74 amu, and its radius is 1.26 Å. These parameters are typical for a range of bonds in organic molecules[37] and are used in this work to represent a generic analyte molecule in MALDI. The same parameters were used previously to model MAPLE[35] of siloxane polymers (e.g., PDMS[38]). When the bond length exceeds 7.7 Å, the chemical bond is broken, leading to fragmentation. After the fragmentation, the interaction between the previously bonded beads is calculated as the one between nonbonded beads. All nonbonded interactions are modeled by the same Morse potential as that for the matrix molecules. Because the united-atom models are used both for matrix molecules and for analyte molecules, a relatively large time step of 2 fs is used in the simulation.

The calculations are performed for a rectangular sample with linear dimensions of 100 × 100 × 900 Å that contains about 62 600 matrix molecules. From 9 to 30 analyte molecules, each composed of 40 beads, are introduced into the sample using a random Monte Carlo procedure and removing the overlapping matrix molecules. The total mass of each analyte molecule is 2960 Da. Before exposure to a laser pulse, the system is quenched. Dynamic boundary conditions are used to eliminate the reflection of the laser induced pressure wave from the bottom of the simulated sample.[39] In the lateral directions, periodic boundary conditions are imposed. Laser irradiation is simulated by vibrational excitation of randomly chosen matrix molecules. The vibrational excitations are performed by depositing a quantum of energy equal to the photon energy into the kinetic energy of internal vibration of the molecules to be excited. The absorption probability decreases exponentially with depth in accordance with Beer's law. The laser penetration depth, L_p, is assumed to be 500 Å, and the laser wavelength is set to be 337 nm. Two values of the laser pulse width, $\tau = 150$ and 300 ps, are used in the simulation. The laser fluence is varied between 10 and 110 J/m^2.

3. Simulation Results and Discussion

In this paper, we present the simulation results obtained with a laser pulse duration corresponding to the thermal-confinement regime, which is typical for UV-MALDI.[20,32] This regime is realized when the pulse duration is longer than the characteristic time of relaxation of the laser-induced stresses, t_p, but shorter than the time of dissipation of the absorbed energy by the thermal conduction, t_{th}. First, we discuss the ablation process and the ablation yield. The degree of solvation of the analyte molecules in the matrix clusters is investigated as a function of laser fluence. In the next subsection, we discuss the mechanisms of the desolvation of analyte molecules. The processes that could lead to analyte fragmentation are addressed in the final part.

3.1. Plume Development and Analyte Ejection. A snapshot of the laser plume obtained in the simulation for a laser fluence above the ablation threshold is shown in Figure 1. The simulations clearly demonstrate that analyte molecules (red) are

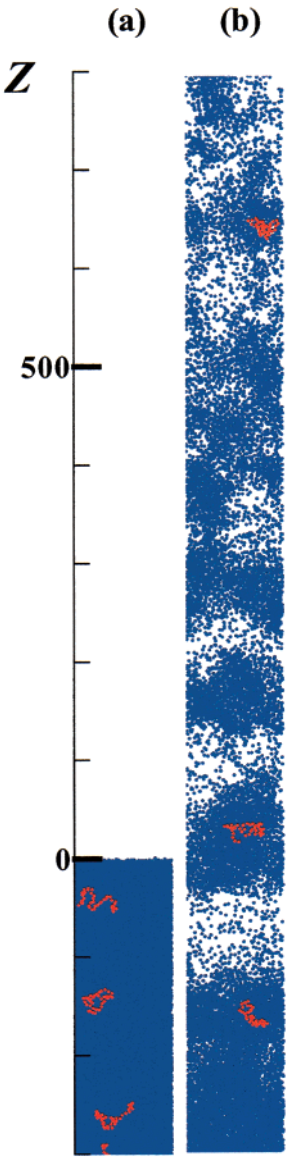

Figure 1. Snapshots from the MD simulation showing a portion of the laser plume obtained with laser pulse width $\tau = 150$ ps and laser fluence $F = 70$ J/m^2. (a) Initial sample, (b) laser plume at $t = 200$ ps after the end of the laser pulse. The Z axis is directed along the outward surface normal, and the position of the irradiated surface corresponds to $z = 0$. For clarity, the analyte molecules (red) are plotted in front of the matrix molecules (blue), whereas in reality, they are inside the sample.

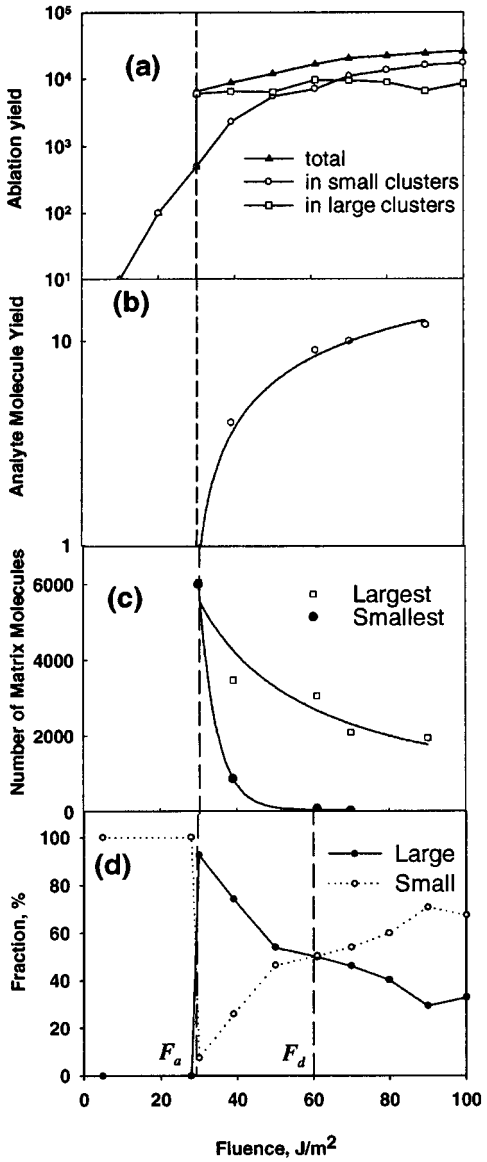

Figure 2. (a) Matrix yield vs laser fluence. Circles represent the number of matrix molecules ejected in the form of monomers and small clusters (four molecules or fewer), squares correspond to the number of matrix molecules ejected in the form of big clusters (more than four molecules), and triangles show the total yield of the matrix molecules. The partitioning between small and large is arbitrary, and any choice of small and large exhibits the same trend. (b) Analyte molecules. (c) Number of matrix molecules in clusters containing one analyte molecule. Squares show the number of matrix molecules attached to the analyte molecule in the largest cluster, whereas solid circles display the one in the smallest cluster. (d) The percentage of matrix molecules in small and large clusters. The data points are obtained $t = 650$ ps after the laser pulse. The vertical line in all frames shows the ablation threshold F_a. Lines in frames b and c are just guides to the eye. The second vertical line in frame d indicates the laser fluence $F_d \sim 2Fa$ at which the fraction of small clusters exceeds the one of big clusters.

entrained in the expanding plume of matrix molecules (blue). The figure also illustrates that, in addition to monomers, the laser plume contains big clusters composed of both matrix and analyte molecules.

A quantitative analysis of analyte ejection relative to the physical mechanisms of ablation is shown in Figure 2. Figure 2a demonstrates the calculated yield of matrix molecules, which is defined in the simulation as a number of molecules ejected at a distance more than 100 Å above the position of the initial irradiated surface. As discussed previously, at low fluences, the removal of material occurs because of desorption.[19,28] For a laser fluence $F_a = 30$ J/m^2 corresponding to the ablation threshold in our simulation, a discontinuity in the total yield can be observed, indicating the transition from the desorption regime to the ablation regime. At this fluence, the amount of the material removed increases because of the explosive boiling of the material overheated by the fast laser energy deposition, which leads to the ejection of molecular clusters.[20,21] Quantitatively, the fluence values are lower in our simulation than in typical MALDI experiments because of the difference in the heat capacity of the irradiated sample, the presence of the reflection losses in experiments, and the difference in optical penetration depth.[21,30] The ejection of analyte molecules occurs only in the ablation regime, i.e., when laser fluence is larger than F_a [Figure 2b]. In this regime, the strong cooperative motion of the ablated

material leads to the ejection of the analyte molecules. The ejection of analyte molecules when the laser fluence is above the ablation threshold agrees with experiments[10,40] and with previous simulations.[29,40]

Our calculations show that the ablated analyte molecules are typically solvated within relatively large clusters of matrix molecules. Figure 2c illustrates the laser fluence dependency of the number of matrix molecules in the largest (moving in the plume tail) and smallest (moving in the front part of the plume) clusters that contain an analyte molecule. One can see in the figure that the size of the smallest cluster diminishes rapidly as the fluence increases up to a value of about twice the ablation threshold.

Clusters of matrix molecules[24,41,42] and clusters of analyte molecules[43−45] are evidently present in many MALDI experiments. Indirect evidence of the ejection of molecular clusters in MALDI has been obtained in postionization[43,40] and the delayed extraction[46] time-of-flight mass spectrometry experiments. Several models of ionization in MALDI assume that the analyte molecules are in close contact with matrix molecules as the plume is evolving.[2,46−49] In general, however, MALDI spectra do not exhibit strong ion signals corresponding to matrix adducts. Having the analyte ion signal partitioned into several peaks is not desirable for an analytical protocol, and at least partially, the absence of the analyte−matrix clusters in a typical MALDI experiment can be attributed to a deliberate choice of matrixes that minimize the clustering of matrix molecules around the analyte ions.[41] Regardless of whether some matrixes under some experimental conditions solvate the analyte ions, there are some conditions under which the analyte ions are not encumbered with matrix molecules. Several physical processes that can lead to desolvation of the analyte molecule are discussed in the next subsection.

Before discussing possible scenarios of the analyte desolvation, we first checked that the analyte−matrix interaction is not too strong in our simulation. To examine this possibility, we have performed a set of simulations scaling down both the parameters of the matrix−analyte and matrix−matrix potential. The only difference observed is that both the ablation threshold and the dependency of the yields are shifted to lower fluences. The analyte molecules are still solvated. It is known from experiments that analyte molecules must be miscible in the original matrix in order to obtain good spectra. Thus, the strength of the matrix−matrix and matrix−analyte interactions must be comparable. Therefore, our choices of parameters are sensible, and the observed solvation of analyte molecules is not an artifact of the simulation. Ongoing simulations of explosive boiling in a system of water molecules with an embedded small peptide molecule also exhibit considerable solvation.[50]

3.2. Desolvation of Analyte Molecules. If analyte molecules are ejected solvated, then how can one explain the observation of isolated analyte molecules in MALDI experiments? The following processes can account for these observations. (i) Under some set of specific conditions, a small fraction of analyte molecules can be ejected without matrix molecules attached to them. (ii) Thermal evaporation of clusters occurs after the end of the laser pulse and before detection. (iii) Desolvation can occur because of collisions of solvated analyte molecules with plume molecules during ion extraction. Below we will consider these processes in more detail. It should be noted, however, that we perform the calculations only until about 1 ns from the end of the laser pulse. The typical time-of-flight of an analyte molecule from the irradiated target to the detector is on the order of microseconds. Therefore, our simulations cannot describe all of the processes leading to the desolvation. In addition, because we do not explicitly consider intramolecular atomic vibrations, the amount of energy that can be accumulated in the model material is smaller than the real heat capacity of a molecular solid.[21] Nevertheless, we qualitatively consider the main mechanisms of the analyte desolvation.

Single Analyte Molecules. One possible explanation for the unsolvated analyte ions is that these ions arise from very special conditions. As shown in Figure 2c,d, our calculations predict that the amount of solvation is less if the analyte molecule is originally close to the surface and if the laser fluence is almost twice the ablation threshold. There have been proposals that the analyte molecule must be on the surface[51] or that the ion formation threshold is well above the ablation threshold. There is also a possibility that the analyte molecules can segregate at grain boundaries of the crystalline matrix. In the simulations presented here, the analyte molecule is embedded into in a very homogeneous environment.

Thermal Evaporation. Because of the high temperature attained at the end of the laser pulse, natural desolvation (or thermal evaporation) of matrix molecules from hot clusters can lead to the liberation of analyte molecules from precursor clusters after the end of the laser pulse. To provide a qualitative description of the matrix−analyte energy transfer, we monitor the internal energy of the analyte molecules as shown in Figure 3a. The internal energy of analyte molecules is calculated as a sum of potential and kinetic energy of analyte beads. The simulation results show that the internal energy rises during the laser pulse and decreases thereafter. The decay of the internal energy after the end of the laser pulse correlates with the process of analyte desolvation (Figure 3b). The observed correlation can be explained by the evaporative cooling that helps in stabilizing the analyte molecules. One can note, furthermore, that the major desolvation takes place after the laser pulse, at the stage when the plume cools because of the phase transition. In fact, the temperature in the plume decreases considerably after the end of the laser pulse during a period which is comparable to the laser pulse width.[20] Earlier, molecular dynamics simulations predicted that at longer laser pulses the ejected clusters are smaller.[20,32] Figure 3c demonstrates also that desolvation is slower when the laser pulse is longer.

Previously, investigations of the evaporation of clusters have been performed by using classical nucleation theory,[53] RRK theory,[54,55] kinetic theory,[56] and molecular dynamics simulation.[53,57] These studies showed that the evaporation rate is typically low. For example, thermal evaporation of an argon cluster containing more than 600 atoms was estimated to continue during a few microseconds.[47] In addition, both the present simulation and previous investigations of cluster evaporation indicate that clusters do not evaporate completely. This result can be attributed to the decrease of cluster temperature because of thermal evaporation.[47] In addition, the frequency of collisions among clusters and plume molecules decreases as a result of the plume expansion. Therefore, the temperature of the clusters, even being higher than the one of the gas component of the plume,[20] decays faster in an expanding plume than in a stationary case. At shorter laser pulses, clusters cool more rapidly after the end of the pulse, and cluster sizes stabilize. For longer laser pulses, the initially smaller clusters cool more slowly, and therefore, clusters can evaporate to a smaller size. However, thermal evaporation seems to be insufficient for complete desolvation, and additional mechanisms must be considered.

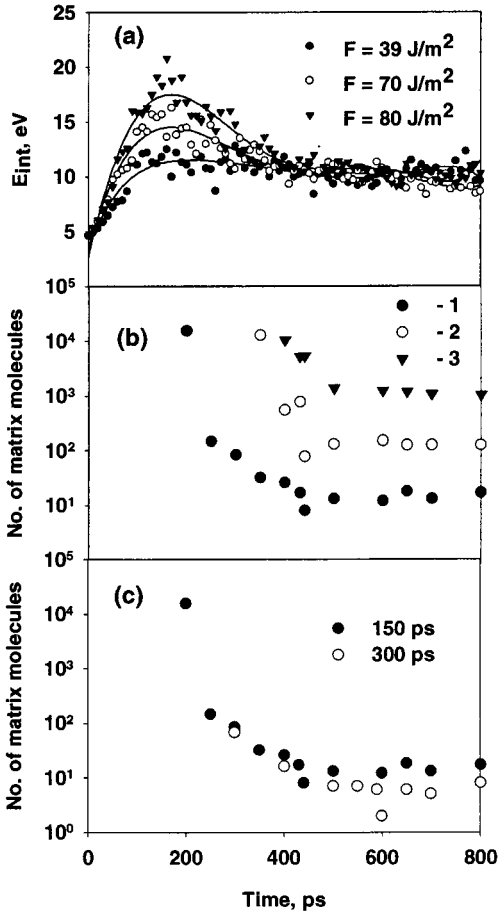

Figure 3. (a) Internal energy of analyte molecules vs time for different laser fluences. Circles correspond to $F = 39$ J/m^2, diamonds correspond to $F = 70$ J/m^2, and triangles correspond to laser fluence $F = 90$ J/m^2. Calculations are performed for pulse duration $\tau = 150$ ps and the number of analyte molecules $N_a = 9$, and the results are shown for the analyte molecule embedded near the irradiated surface. (b) Number of matrix molecules in the clusters containing analyte molecules as a function of time. The initial positions of the analyte molecules are (1) $Z_0 = -42.3$ Å (the smallest cluster containing an analyte molecule), (2) $Z_0 = -143$ Å, and (3) $Z_0 = -262$ Å (the biggest cluster containing an analyte molecule). (c) Same as b for the smallest cluster and two laser pulse width $\tau = 150$ and 300 ps.

Gas-Phase Collisions during Ion Extraction. In the presence of an electric field, additional processes can lead to analyte desolvation. In this case, small charged clusters containing analyte molecules will undergo many collisions with plume molecules during their extraction in the electric field. Because matrix molecules are more weakly bound to the analyte molecules than the bonding interactions within the analyte molecule, the collisions within the plume can result in the liberation of analyte molecules from the matrix. Supporting this hypothesis, several experiments demonstrated that the energy of the extracted analyte ions is smaller than one would expect from the acceleration in the electric field.[9,58] For example, the energy deficit of 24 eV was reported for insulin ions by Zhou et al.[9] The revealed energy deficit was attributed to the collisions with the neutral species in the plume during the extraction. These results indicate that an amount of energy transferred to a charged cluster during the extraction could be sufficient to increase the cluster temperature and to promote the desolvation. Additional collision effects can also lead to the liberation of the analyte molecules from the matrix when experiments are performed in the presence of a low-pressure buffer gas.[59]

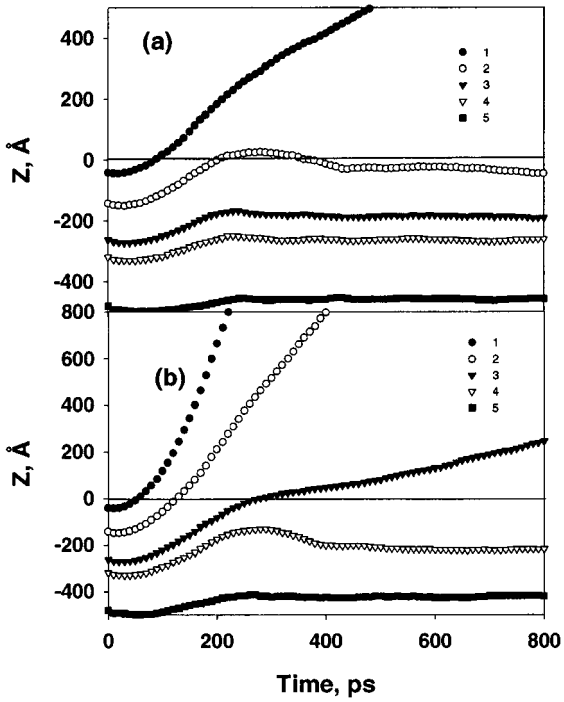

Figure 4. Z positions of the center of mass of the analyte molecules initially embedded at different depths as a function of time. The numbers correspond to the different analyte molecules initially embedded at different depth, (1) $Z_0 = -42$ Å, (2) $Z_0 = -149$ Å, (3) $Z_0 = -262$ Å, (4) $Z_0 = -314$ Å, and (5) $Z_0 = -480$ Å. (a) Simulation results for laser pulse duration $\tau = 150$ ps and laser fluence $F = 39$ J/m^2. (b) Simulation results for laser pulse duration $\tau = 150$ ps and laser fluence $F = 70$ J/m^2. The Z axis is directed along the outward surface normal, and $Z = 0$ corresponds to the initial position of the irradiated surface.

In this part, we have discussed the major mechanisms that can account for the observation of isolated analytes. Calculation results have shown that natural desolvation is a slow process, which can give rise only to a partial desolvation. The desolvation mechanism is most probably promoted by collisional interaction of clusters with plume molecules at the initial stage of the plume development and during the ion extraction.

3.3. Velocities and Fragmentation of Analyte Molecules. The movement of the analyte molecules away from the surface is illustrated in Figure 4. At a laser fluence just above the ablation threshold [Figure 4a], only the analyte molecule initially located close to the irradiated surface is ejected. With the increase in fluence, more analyte molecules are entrained in the plume [Figure 4b]. The molecules that are initially embedded deeper under the irradiated surface start moving later and are slower than the ones that are embedded closer to the irradiated surface. These results can be related to the effect of entrainment of analyte molecules and molecular clusters that was observed earlier.[20,29] Free expansion of the plume leads to the linear dependency of the flow velocity on the distance from the initial surface. The analyte molecules are entrained into the expanding plume and move along with the individual molecules with nearly the same velocities. Therefore, analyte molecules that are in the tail of the plume are slower than the ones in the front part of the plume.[29] The analyte center-of-mass velocities are proportional to the slope of the $Z_i(t)$ curves. The velocities of the ejected analyte molecules range from 40 to 1200 m/s and increase with laser fluence. These values are comparable to those from a number of experiments in which velocities in the range of 500−1200 m/s are measured.[9,58,60−65]

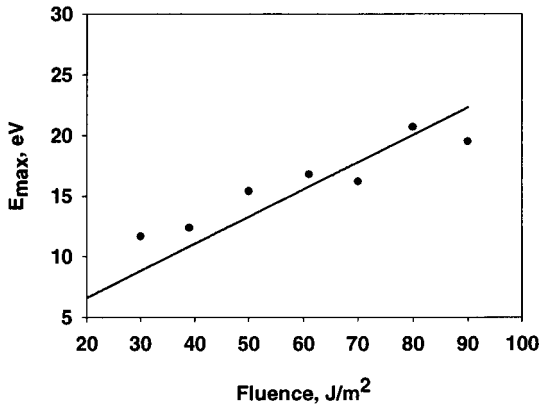

Figure 5. Maximum value of the internal energy of that analyte molecule embedded at the depth $Z_0 = -42$ Å as a function of laser fluence. Calculation results are obtained at $t = \tau = 150$ ps. The line is a linear fit to the dependency.

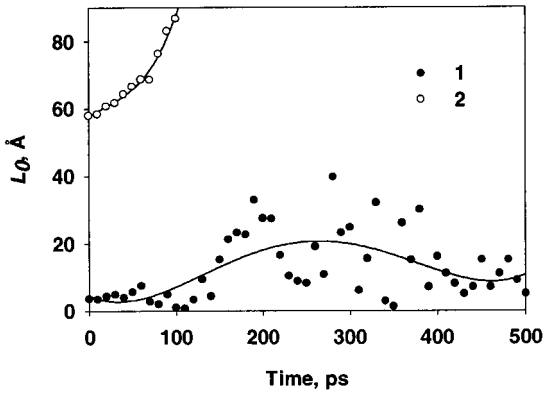

Figure 6. Distance between the end beads of the analyte molecule (the length, l_0) as a function of time. Calculations are performed for laser pulse duration $\tau = 300$ ps and laser fluence $F = 90$ J/m^2. (1) the molecule is initially unextended; (2) the analyte molecule is initially extended in the direction perpendicular to the irradiated surface. At $t = 110$ ps the first molecule is broken. Lines are just guides to the eye.

Typical MALDI-TOF experiments show a deterioration of the mass spectra at high laser fluences. This result is frequently attributed to the fragmentation of molecules, because the formation of fragments with different molecular weight decreases the resolution of the MALDI−TOF technique.[2] There can be two main reasons of analyte fragmentation, (i) the increase in temperature (thermal effects) and (ii) mechanical stress.

For fragmentation due to thermal effects, the internal energy of the analyte molecule should exceed a certain dissociation threshold value. The exact calculation of the threshold is not possible within the bead-and-spring approximation. An estimate can be obtained from classical RRK theory, in which the molecule is represented by s oscillators.[66] For example, for molecules with $s = 40$ (the number of spring connectors in each analyte molecule in our simulation) and a bond dissociation energy of 4.6 eV, this estimate gives an internal energy threshold of about 63 eV. We have calculated the maximum internal energy of analyte molecules as a function of laser fluence (Figure 5). From the linear extrapolation of the obtained dependency, one can estimate that $E_{int} \sim 63$ eV at fluences as high as about 290 J/m^2. At these high fluences, the energy absorbed per matrix molecule would be much higher than the average cohesive energy (0.6 eV per molecule in our simulation). The fluence required for the fragmentation is much larger that the one needed for the ejection and liberation of the analyte molecules. The degree of fragmentation is, therefore, negligible at laser fluences typical for MALDI. The solvation of analyte molecules also helps in preventing their fragmentation. In effect, the analytes can transfer the energy stored in their vibrational modes to the surrounding matrix molecules. In addition, collisions with the plume molecules during the extraction only weakly affect solvated analyte molecules and cannot lead to their fragmentation.

The difference in the velocities of the material ejected from different depths in the irradiated sample can also cause analyte fragmentation. To study the structural modifications of analyte molecules, we monitor the time variation of the analyte length (distance between the ending beads) for analyte molecules located close to the irradiated surface (Figure 6). In the first case, the length of the analyte is quite short at the beginning of the laser pulse. In the second case, the analyte molecule is initially extended in the direction perpendicular to the surface. One can see that the length increases during the laser pulse and then decreases in the first case. In the second case, the length of the chain increases rapidly with time until the chain is broken at $t \sim 100$ ps. The observed unfolding and fragmentation of the chain can be explained by the difference in the velocities of the different parts of the molecule entrained in the plume. The velocities of the molecules entrained in the plume are nearly the same as the velocity of the corresponding part of the plume. Different parts of the same molecule, which are situated at different depth, can thus acquire different velocities. The difference in the velocities leads to the unfolding of the molecules during the laser pulse. The unfolding is more pronounced for molecules that are initially more extended in the direction of the plume expansion. The observed unfolding can result in the fragmentation of analyte molecules initially located close to the irradiated surface and parallel to the pressure gradient. We note, however, that in most of the simulations the analyte molecules remain intact as their initial configurations are more compact.

4. Summary

We have presented a numerical investigation of matrix-assisted laser desorption of analyte molecules. Molecular dynamics simulations have been used to elucidate microscopic mechanisms of the analyte molecule ejection and their structural modification. A combination of the breathing sphere model with the bead-and-spring approach has been developed, which allows calculations with large time step and system size.

The simulation results show that analyte molecules are ejected from the surface at laser fluences higher than the laser ablation threshold. The velocity of the ejected high molecular weight analyte molecules can be as high as 1200 m/s. Analytes incorporated closer to the irradiated surface are lifted off at fluences just above the ablation threshold. To eject analyte molecules embedded deeper under the surface, higher fluences are needed. As the laser fluence increases, the yield of both analyte and matrix molecules grows logarithmically.

Our calculations have demonstrated that analyte molecules are ejected within clusters of matrix molecules and are thus solvated. These results support the earlier suggestions of Karas and Hillenkamp[5,7] that the absorption of laser radiation leads to the ejection of large particles of matrix material containing analyte molecules. The calculations show, furthermore, that the number of matrix molecules attached to the analyte molecules is smaller for analyte molecules embedded closer to the surface. In addition, the degree of solvation is found to diminish with laser fluence. The least solvated analyte molecules are, therefore,

those that are embedded near the surface and ejected at a high laser fluence. How the analyte molecules lose all the matrix molecules to be detected as isolated analyte ions in MALDI experiments is still an open question.

Several possible mechanisms of analyte desolvation have been discussed. Two major explanations of the observation of isolated analytes have been suggested. First, thermal evaporation leads to the decrease of cluster's size after the end of the laser pulse. Thermal evaporation, however, can account only for a partial desolvation. Therefore, the mechanism of the desolvation is probably related to collisions of clusters with individual molecules in the plume. These collisions take place both at the initial stage of the plume development and during the analyte extraction by an external electric field. The collisions lead to an increase in the cluster internal energy and to the dissociation of weakly bonded matrix molecules.

The internal energy of analyte molecules is shown to increase during the laser pulse and decrease afterward. The maximum internal energy, which is attained at the end of the laser pulse, rises with laser fluence. The energy is, however, insufficient for the fragmentation of the molecules at all considered laser fluences.

Analytes embedded deeper in the sample have smaller velocities than the ones embedded closer to the irradiated surface. Both the depth dependence of the velocities of the analyte molecules and their structural modifications can be explained by the effect of entrainment of analyte molecules in the plume. In fact, different parts of the same analyte molecule move with nearly the same velocities as matrix molecules in the corresponding part of the plume. Because of the difference in velocities, the molecule unfolds. The molecules located just below the irradiated surface unfold more than the ones that are incorporated deeper and have a globular configuration at the beginning of the simulation. The degree of fragmentation is, however, negligible for most common laser parameters and initial analyte configurations.

Acknowledgment. This work was supported by the United States Office of Naval Research through the Medical Free Electron Laser Program and by the National Science Foundation through the Chemistry Division. The computational support was provided by IBM through the Selected University Research Program, the National Science Foundation through the MRI Program, and the Center for Academic Computing at Penn State University. We thank Yaroslava Yingling for insightful discussions. We are also grateful to Tracy Schoolcraft and Arnaud Delcorte for suggestions on the manuscript.

References and Notes

(1) Karas, M. Fundamental Processes. In *Sputtering of Atoms and Molecules*; Sigmund, P., Ed.; Det Kongelige Danske Videnskabernes Selskab: Copenhagen, 1993.

(2) Karas, M.; Bachmann, D.; Bahr, U.; Hillenkamp, F. *Int. J. Mass Spectrom. Ion Processes* **1987**, *78*, 53.

(3) Tanaka, K.; Waki, H.; Ido, Y.; Akita, S.; Yoshida, Y. *Rapid Commun. Mass Spectrom.* **1988**, *2*, 151.

(4) Karas, M.; Bachmann, D.; Bahr, U.; Hillenkamp, F. *Anal. Chem.* **1988**, *60*, 2299.

(5) Karas, M.; Hillenkamp, F. *Anal. Chem.* **1988**, *60*, 229.

(6) Karas, M.; Bahr, U.; Hillenkamp, F. *Int. J. Mass Spectrom. Ion Processes* **1989**, *92*, 231.

(7) Spengler, B.; Karas, M.; Bahr, U.; Hillenkamp, F. *Ber. Bunsen-Ges. Phys. Chem.* **1989**, *93*, 396.

(8) Ens, W.; Mayer, Y.; Standing, K. G. *Rapid Commun. Mass Spectrom.* **1991**, *5*, 117.

(9) Zhou, J.; Ens, W.; Standing, K. G.; Verenchikov, A. *Rapid Commun. Mass Spectrom.* **1992**, *6*, 671.

(10) Dreisewerd, K.; Schürenberg, M.; Karas, M.; Hillenkamp, F. *Int. J. Mass Spectrom. Ion Processes* **1995**, *141*, 127.

(11) Brown, R. S.; Feng, J.; Reiberg, D. C. *Int. J. Mass Spectrom. Ion Processes* **1995**, *169/170*, 1.

(12) Schriemer, D. C.; Li, L. *Anal. Chem.* **1996**, *68*, 2721; **1997**, *69*, 4169.

(13) Fenselau, C. *Anal. Chem.* **1997**, *69*, 661A−665A.

(14) Berkenkamp, S.; Karas, M.; Hillenkamp, F. *Proc. Natl. Acad. Sci. U.S.A.* **1996**, *93*, 7003.

(15) Piqué, A.; Mcgill, R. C. R. A.; Chrisey, D. B.; Callahan, J.; Mlsna, T. E. *Mater. Res. Soc. Symp. Proc.* **1998**, *526*, 375.

(16) Bencsura, A.; Navale, V.; Sadeghi, M.; Vertes, A. *Rapid Commun. Mass Spectrom.* **1997**, *11*, 679.

(17) Vertes, A.; Juhasz, P.; DeWolf, M.; Gijbels, R. *Scanning Microsc.* **1988**, *2*, 1853.

(18) Benscura, A.; Vertes, A. *Chem. Phys. Lett.* **1995**, *247*, 142.

(19) Johnson, R. E. In *Large Ions: Their Vaporization, Detection and Structural Analysis*; Baer, T., Ng, C. Y., Powis, I., Eds.; John Wiley: New York, 1996; p 49.

(20) Zhigilei, L. V.; Garrison, B. J. *J. Appl. Phys.* **2000**, *88*, 1281.

(21) Zhigilei, L. V.; Garrison, B. J. *J. Appl. Phys. Lett.* **1999**, *74*, 1341.

(22) Domen, K.; Chuang, T. *J. Phys Rev Lett.* **1987**, *59*, 1484.

(23) Garrison, B. J.; Srinivasan, R. *Appl. Phys. Lett.* **1984**, *44*, 849−851.

(24) Handschuh, M.; Nettesheim, S.; Zenobi, R. *Appl. Surf. Sci.* **1999**, *137*, 125.

(25) Wu, X.; Sadeghi, M.; Vertes, A. *J. Phys. Chem. B* **1998**, *102*, 4770.

(26) Sadeghi, M.; Wu, X.; Vertes, A. *J. Phys. Chem. B* **2001**, *105*, 2578.

(27) Zhigilei, L. V.; Kodali, P. B. S.; Garrison, B. J. *J. Phys. Chem. B.* **1997**, *101*, 2028.

(28) Zhigilei, L. V.; Kodali, P. B. S.; Garrison, B. J. *J. Phys. Chem. B.* **1998**, *102*, 2845.

(29) Zhigilei, L. V.; Garrison, B. J. *Rapid Commun. Mass Spectrom.* **1998**, *12*, 1273.

(30) Zhigilei, L. V.; Garrison, B. J. *Appl. Phys. Lett.* **1997**, *71*, 551.

(31) Zhigilei, L. V.; Kodali, P. B. S.; Garrison, B. J. *Chem. Phys. Lett.* **1997**, *276*, 269.

(32) Zhigilei, L. V.; Garrison, B. J. *Appl. Phys. A.* **1999**, *69*, S75.

(33) Öttinger, H. C. *Stochastic Processes in Polymeric Fluids*; Springer-Verlag: Berlin, 1996.

(34) Cascales, J. J. L.; Díaz, F. G.; García de la Torre, J. *Polymer* **1995**, *36* (2), 345.

(35) Itina, T. E.; Zhigilei, L. V.; Garrison, B. J. *Nucl. Instrum. Methods B* **2001**, *180*, 238.

(36) Dou, Y.; Zhigilei, L. V.; Winograd, N.; Garrison, B. J. *J. Phys. Chem. A* **2001**, *105*, 2748.

(37) *Handbook of Chemistry and Physics*; Weast, R. C., Ed.; The Chemical Rubber Co: Boca Raton, FL, 1968.

(38) Clarson, S. J.; Semlyen, J. A. *Siloxane Polymers*; PTR Prentice Hall: Englewood Clifs, NJ, 1993.

(39) Zhigilei, L. V.; Garrison, B. J. Multiscale Modelling of Materials. *Mater. Res. Soc. Symp. Proc.* **1999**, *538*, 491.

(40) Yingling, Y. G.; Zhigilei, L. V.; Garrison, B. J.; Koubenakis, A.; Labrakis, J.; Georgiou, S. *Appl. Phys. Lett.* **2001**, *78*, 1631.

(41) Russell, D. H. Private communication, 2001.

(42) Song, K.; Xu, X. *Appl. Surf. Sci.* **1998**, *127−129*, 11.

(43) Hankin, S. M.; John, P. *J. Phys. Chem B* **1999**, *103*, 4566.

(44) Kinsel, G. R.; Gimon-Kinsel, M. E.; Gilling, K. J.; Russell, D. H. *J. Mass Spectrom.* **1999**, *34*, 684.

(45) Strobel, F. H.; Preston, L. M.; Washburn, K. S.; Russell, D. H. *Anal. Chem.* **1992**, *64*, 754.

(46) Fournier, I.; Brunot, A.; Tablet, J. C.; Bolbach, G. Private communications, 2001.

(47) Karas, M.; Glückmann, M.; Schäfer, J. *J. Mass Spertrom.* **2000**, *35*, 1.

(48) Zenobi, R.; Knochenmuss, R. *Mass Spectrom. Rev.* **1999**, *17*, 337.

(49) Karbach, V.; Knochenmuss, R. *Rapid Commun. Mass Spectrom.* **1998**, *12*, 968.

(50) Dou, Y.; Zhigilei, L. V.; Winograd, N.; Garrison. B. J. Private communications.

(51) Cohen, L. R. H.; Strupat, K.; Hillenkamp, F. *J. Am. Soc. Mass Spectrom.* **1997**, *8*, 1039.

(52) Reference deleted in revision.

(53) Bedanov, B. M.; Gadiak, G. V. *Modeling in Mechanics*; The Institute of Theoretical and Applied Mechanics: Novosibirsk, Russia, 1987; Vol. 1, p 13, in Russian.

(54) Haberland, H., Ed.; *Clusters of Atoms and Molecules*; Springer: Berlin, 1994; p 207.

(55) Malahovskii, A. V.; Ben-Zion, M. *Chem Phys.* **2001**, *264*, 135.

(56) Davies, C. N. Evaporation of airborne droplets. In *Fundamentals of aerosol science*; Shaw, D. T., Ed.; Wiley: New York, 1978; Chapter 3, p 155.

(57) Thompson, S. M.; Gubbins, K. E.; Walton, J. P. R. B.; Chantry, R. A. R.; Rowlinson, J. S. *J. Chem. Phys.* **1984**, *81* (1), 530.

(58) Juhasz, P.; Vestal, M. L.; Martin, S. A. *J. Am. Soc. Mass Spectrom.* **1997**, *8*, 209.
(59) Gilling, K. J.; Ruotolo, B.; Stone, E. G.; Russell, D. H.; Fuhrer, K.; Gonin, M.; Schultz, A. *J. Anal. Chem.* **2000**, *72*, 3965.
(60) Kinsel, G. R.; Edmondson, R. D.; Russell, D. H. *J. Mass Spectrom.* **1997**, *32*, 714.
(61) Kinsel, G. R.; Gimon-Kinsel, M. E.; Gillig, K. J.; Russell, D. H. *J. Mass Spectrom.* **1999**, *34*, 684.
(62) Elam, J. W.; Levy, D. H. *J. Phys. Chem. B* **1998**, *102*, 8113.
(63) Glückman, M.; Karas, M. *J. Mass Spectrom.* **1999**, *34*, 467.
(64) Pan, Y.; Cotter, R. J. *Org. Mass Spectrom.* **1992**, *27*, 3.
(65) Huth-Fehre, T.; Becker, C. H. *Rapid Commun. Mass Spectrom.* **1991**, *5*, 378.
(66) Robinson, P. J.; Holbrook, K. A. *Unimolecular Reactions*; Wiley, New York, 1972.